The Influence of Solution Anion on the Mechanism of Transpassive Dissolution of Ferrous- and Nickel-Based Alloys

Martin Bojinov*,† and Tzvety Tzvetkoff‡

VTT Technical Research Centre of Finland, P.O. Box 1704, FIN-02044 VTT, Espoo, Finland, and Department of Physical Chemistry, University of Chemical Technology and Metallurgy, 1756 Sofia, Bulgaria

Received: January 10, 2003; In Final Form: February 24, 2003

The aim of this work is to generalize the model for the transpassive dissolution of ferrous- and nickel-based alloys in acidic solutions by assessing the effect of the solution anion on the individual steps of the process. First, experimental voltammetric and impedance spectroscopic data on transpassive dissolution of pure Cr, Fe−12%Cr, Fe−12%Cr−5%Mo, Fe−25%Cr, Fe−25%Cr−10%Mo, pure Ni, Ni−10%Cr, and Ni−20%Cr in phosphoric acid solution are compared with earlier data for the same materials in sulfuric acid solution. It is found that phosphate affects mainly the dissolution reaction of the main element (Fe and Ni) significantly enhancing the rate of secondary passivation in comparison to sulfate. In addition, the accelerating effect of Mo on transpassive dissolution of Cr is much less pronounced in phosphate solutions. Second, the physicochemical basis of the generalized kinetic model is described. The additional assumptions and simplifications that are necessary to transform the model into a set of kinetic equations are listed, and the individual models for the transpassive dissolution of ferrous- and nickel-based alloys are presented. The kinetic parameters of the transpassive dissolution process in 1 M H_3PO_4 are determined and compared to those in 1 M H_2SO_4 published earlier. Finally, some conclusions on the effect of solution anion on transpassive dissolution are drawn, and the limitations of the models are outlined.

1. Introduction

The fundamental understanding of general and localized corrosion phenomena in highly oxidizing environments encountered in the process industry and during surface treatment of engineering alloys requires detailed information on the interaction of the passive film formed on these materials and ionic species present in the surrounding electrolytic medium. In such environments, there appears to be a competition between localized corrosion caused by anions such as chloride and general corrosion resulting from the dissolution of alloyed Cr and Mo in the so-called transpassive state.[1−3]

Transpassive dissolution of alloys is a complex process, involving the following reaction steps: (1) oxide film growth by generation, transport, and consumption of anion vacancies coupled to chemical dissolution of the film to preserve a steady-state thickness; (2) dissolution of the alloy constituents through the film by generation, transport, and consumption of cation vacancies or interstitial cations or both; (3) further oxidation of cations or cation−anion interaction at the film/solution interface; (4) transport of soluble products in the bulk solution. In principle, anions from the solution can exert an influence over most of the reaction stages. They are incorporated to a certain extent in the growing passive film[4] and have been proposed to form ion-vacancy pairs thus altering the distribution of point defects in the film.[5] Thus anions from the solution can influence the solid-state reactions of oxidation of cations in the film to a higher valency state. Further, they can facilitate the extraction of cations, for example, Fe or Ni, from the film at its interface with the electrolyte by forming highly soluble aqueous complexes with such cations.[6] Alternatively, they can stabilize the film by suppressing the dissolution via the formation of sparingly soluble species and promote secondary passivation. It can be concluded that solution composition is one of the key factors determining the extent of transpassive dissolution from engineering alloys in the industrial practice.[6]

General theories of the transpassive state[7−9] assume that it is caused by oxidation of a cation to a higher valency state than that in the primary passive film. In ferrous alloys, transpassive dissolution results in an impoverishment of Cr and Mo in the outermost cation layer of the passive film.[10−14] Accordingly, a secondary passive state is reached in which the overall reaction rate is limited by the rate of isovalent dissolution of the main element (Fe) through the film.[10−14] The rate of this process, and hence the efficiency of secondary passivation, is significantly influenced by the solution pH and the type of the solution anion.[15,16]

However, the well-known phenomenon of the transpassivity of Ni cannot be described according to such a theory because it has been established that the dissolution valency of Ni does not increase in the transpassive region.[17] In this particular case, cation−anion interaction at the passive film/solution interface has been invoked to explain the transformation of Ni cations to an activated more soluble form that accelerates dissolution in an autocatalytic step.[17] This process is expected to be strongly influenced by the type of anion present in the electrolyte. In that kind of mechanism, secondary passivation has been ascribed to the formation of a higher-valency Ni with considerably lower solubility at the interface.[17]

In summary, it becomes evident that the extent of transpassive dissolution and secondary passivation of metals and alloys is significantly dependent on the solution composition. The present

* To whom correspondence should be addressed. Phone +358-9-456 5873. Fax: +358-9-456 5875. E-mail: martin.bojinov@vtt.fi.
† VTT Technical Research Centre of Finland.
‡ University of Chemical Technology and Metallurgy.

10.1021/jp0340616 CCC: $25.00
Published on Web 04/30/2003

work addresses the problem by comparing the transpassive dissolution of a range of ferrous- and nickel-based alloys in 1 M solutions of phosphoric and sulfuric acid. Both voltammetric and impedance spectroscopic measurements are employed to characterize the individual reaction steps detectable by electrochemical means. First, we focus on the comparison between the experimental results obtained in the two solutions with an emphasis on the common points and the dissimilarities between the transpassive dissolution features as depending on the alloy composition. Next, a generalized kinetic model is proposed to explain the experimental results. A procedure of determination of the kinetic parameters is outlined and a discussion of their relevance with respect to the influence of solution anion on the transpassive dissolution process is presented.

2. Experimental Section

2.1. Electrodes and Electrolytes. High-purity Fe−12%Cr, Fe−12%Cr−5%Mo, Fe−25%Cr, Fe−25%Cr−10%Mo (Institute of Metal Science, Bulgarian Academy of Sciences), Ni−10%Cr, and Ni−20%Cr (Goodfellow), as well as pure Ni (99.9%, Goodfellow) and Cr (99.7%, Goodfellow), were used as working electrode materials. They were embedded in polytetrafluoroethylene (PTFE) holders and insulated with epoxy resin to expose an area of 0.2 cm^2 to the electrolyte and mounted on a rotating disk electrode setup. Their pretreatment consisted of wet mechanical polishing with emery papers up to grade 4000 followed by a 3 μm alumina to obtain a mirror finish, washing with acetone, and drying with hot air. A conventional three-electrode glass cell was used featuring a Pt plate (area ca. 10 cm^2) as a counter electrode and a saturated calomel electrode as a reference. All of the potentials in the paper are given in the standard hydrogen electrode (SHE) scale. The electrolytes were prepared from 97% H_2SO_4 (Merck) or 85% H_3PO_4 (Riedel-de-Haen) and ultrapure water. Measurements were performed at room temperature in naturally aerated solutions (no influence of nitrogen purging on the results was found in preliminary work).

2.2. Apparatus and Procedure. An Autolab PGSTAT 30 potentiostat equipped with a FRA2 module and driven by GPES 4.9 and FRA 4.9 software (Eco Chemie, The Netherlands) was used for both voltammetric and ac impedance measurements. Current vs potential curves were registered typically at a sweep rate of 1 mV s^{-1} and a rotation rate of 600 rpm following a prepolarization in the passive region (at 1.04 V) for 1 h. No effect of rotation rate (300−1800 rpm) on the voltammetric curves was detected within the reproduciblity limit (±5%). Impedance spectra were registered in the transpassive region (1.14−1.84 V) at 50 or 100 mV intervals after a steady state was reached (criterion, current variation during a measurement ≤ 2%). All of the potential values were corrected by the IR drop calculated from the steady-state current and the high-frequency intercept of the impedance spectra. The frequency range was typically between 20 kHz and 0.01 Hz at an ac amplitude of 10 mV (rms). No influence of the signal amplitude in the range 2−20 mV was detected within the reproducibility limit of the impedance (±3% by magnitude and ±4° by phase). The causality of the systems was checked by a Kramers−Kronig transform test of selected impedance data included in the FRA 4.9 software.

3. Results

3.1. Ferrous Alloys. *3.1.1. Voltammetric Measurements.* Figure 1 summarizes the voltammetric behavior of the studied ferrous alloys during transpassive dissolution in 1 M H_2SO_4 (a) and H_3PO_4 (b). As discussed in previous papers,[13,14,18] the curves can be divided basically in two regions—a region of a fast increase of the current (1.2−1.3 V), that is, a transpassive dissolution region, and a region in which the dependence of the current on potential either becomes less pronounced or altogether vanishes (secondary passivation region, 1.3−1.7 V). In sulfuric acid solution, the tendency toward secondary passivation, as evidenced by the appearance of a plateau in the current vs potential curves, decreases as the content of Cr and Mo in the alloy increases. Moreover, the plateau current for the Fe−12%Cr−5%Mo alloy is almost an order of magnitude greater than that on Fe−12%Cr (Figure 1a). Accordingly, the secondary passivation features for the alloys containing 25% Cr are seen only as a decrease of the slope of the current vs potential curve (Figure 1a).

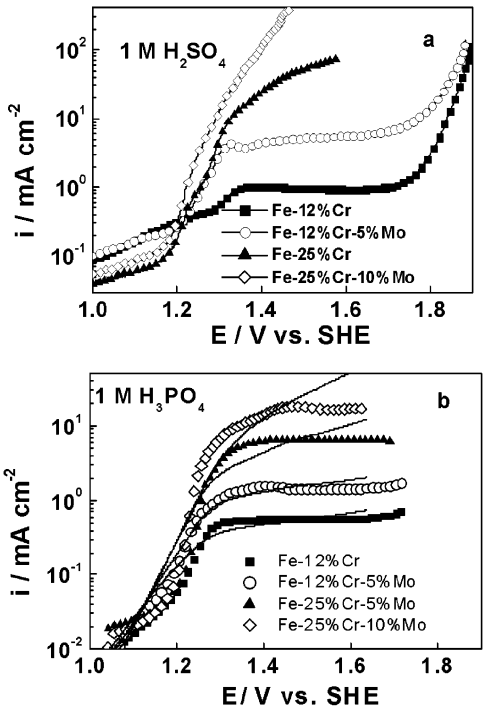

Figure 1. Current vs potential curves for the studied ferrous alloys in (a) 1 M H_2SO_4 and (b) 1 M H_3PO_4. Sweep rate = 1 mV s^{-1}; rotation rate = 600 rpm; points = experimental values; solid lines = best-fit calculation according to the proposed kinetic model.

A comparison of the curves measured in 1 M H_3PO_4 with those in 1 M H_2SO_4 shows that a plateau region is detected for all of the materials in 1 M H_3PO_4 and the currents in the potential region 1.3−1.7 V are considerably smaller in the phosphoric acid solution (Figure 1a,b). These observations clearly indicate an important role of the solution anion in the secondary passivation region, where it is expected that the dissolution rate is controlled by the rate of ejection of the cations of the main element, Fe, from the film into the electrolyte.[10−14,18] On the contrary, the effect of both alloy and solution composition in the transpassive dissolution region, where the process is presumed to be controlled by the oxidative dissolution of Cr from the alloy as Cr(VI), is significantly smaller (Figure 1).

3.1.2. Electrochemical Impedance Spectroscopic Measurements. Because the impedance response of the studied alloys in 1 M H_2SO_4 has been discussed in detail elsewhere,[13,14,18] a collection of such data is presented here for comparative purposes only. Figure 2 shows a comparison of the impedance spectra of Fe−12%Cr registered during transpassive dissolution in the two electrolytes, whereas analogous data for Fe−12%Cr−

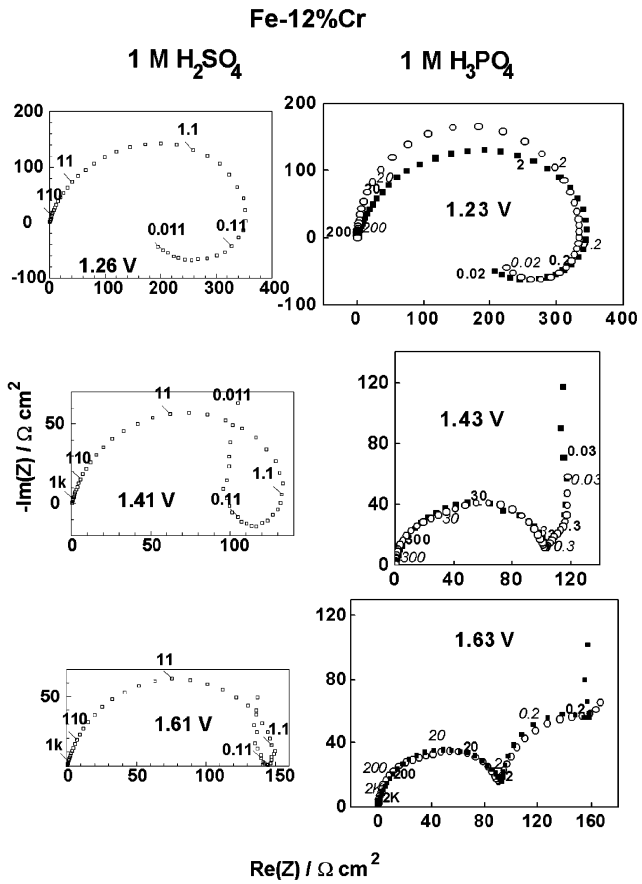

Figure 2. Impedance spectra of the Fe−12%Cr alloy in (left column) 1 M H_2SO_4 and (right column) 1 M H_3PO_4. Parameter is frequency in Hz. In the right column, full symbols are experimental values and empty symbols are best-fit calculation according to the proposed kinetic model.

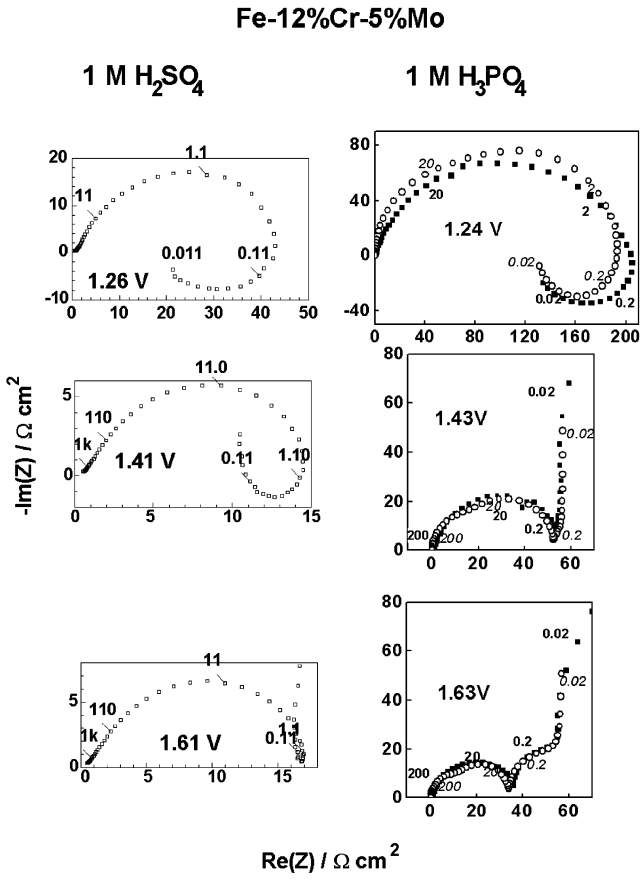

Figure 3. Impedance spectra of the Fe−12%Cr−5%Mo alloy in (left column) 1 M H_2SO_4 and (right column) 1 M H_3PO_4. Parameter is frequency in Hz. In the right column, full symbols are experimental values and empty symbols are best-fit calculation according to the proposed kinetic model.

5%Mo, Fe−25%Cr, and Fe−25%Cr−10%Mo are presented in Figures 3, 4, and 5, respectively. Spectra for pure Cr in the two media are shown in Figure 6.

In the transpassive dissolution region (at ca. 1.25 V), the spectra for all four alloys and pure Cr in the two solutions are qualitatively similar (Figures 2a−6a). This fact is in accordance with the voltammetric results in which no significant difference between the alloys is observed in this potential range (Figure 1). The spectra are composed of a high-frequency capacitive loop and a stretched pseudoinductive low-frequency part, which can be deconvoluted into two overlapped inductive loops.[9] The high-frequency loop has been ascribed to a combination between the impedance of the passive film and the charge-transfer reaction at the film/solution interface.[13,14] The inductive loops have been interpreted as being due to the relaxation of the concentration of negative current carriers in the film and a relaxation of the surface coverage of an intermediate, both accelerating the transpassive dissolution in the transient regime.[13,14]

As the potential increases and enters to the secondary passivation region, however, significant differences are found among different alloys and the influence of the solution anion (phosphate vs sulfate) is clearly detected. For the Fe−12%Cr in 1 M H_2SO_4 (Figure 2, left column), only a low-frequency capacitive feature is added to the spectrum above 1.3 V. Such a low-frequency feature has been earlier interpreted as being due to the modulation of film thickness by the ac signal at constant potential.[18] For Fe−12%Cr in the phosphoric acid solution, on the other hand, the inductive loop vanishes at potentials higher than 1.40 V and a further capacitive loop at ca. 0.2−0.3 Hz is observed (Figure 2, right column). This loop has been connected previously to the relaxation of the surface coverage by an intermediate decelerating the transpassive dissolution rate in the transient regime, that is, causing secondary passivation.[13,14,18] The prominence of the low-frequency capacitive loop in 1 M H_3PO_4 may mean a stabilization of the intermediate product giving rise to secondary passivity in this solution. For the Fe−12%Cr−5%Mo, no qualitative changes in the impedance diagrams are observed with respect to Fe−12%Cr in both solutions (cf. Figures 2 and 3). However, the decrease in the impedance for the Mo-containing alloy in comparison to the Mo-free material is much more dramatic in sulfuric than in phosphoric acid solution (Figure 3). This observation is in accordance with the increase of the current in the voltammetric curves for the Mo-containing alloy over that of the Mo-free alloy (Figure 1). Such a behavior points to a much less pronounced accelerating effect of Mo on the transpassive dissolution of Fe−12% Cr in phosphoric acid solution when compared to that in 1 M H_2SO_4.

In the secondary passivation region, the magnitude of the impedance at low frequencies for the Fe−25%Cr alloy is considerably higher in phosphoric acid solution than in 1 M H_2SO_4, implying a lower reaction rate close to the steady state in accordance to the voltammetric results (Figure 1). For the Fe−25%Cr alloy, the low-frequency capacitive loop appears in general earlier and is much more pronounced in 1 M H_3PO_4 than in 1 M H_2SO_4 (Figure 4). This capacitive loop becomes dominant in the impedance response of the alloy in phosphoric acid solution at higher potentials, and accordingly, the low-frequency inductive loop observed in 1 M H_2SO_4 is not detected

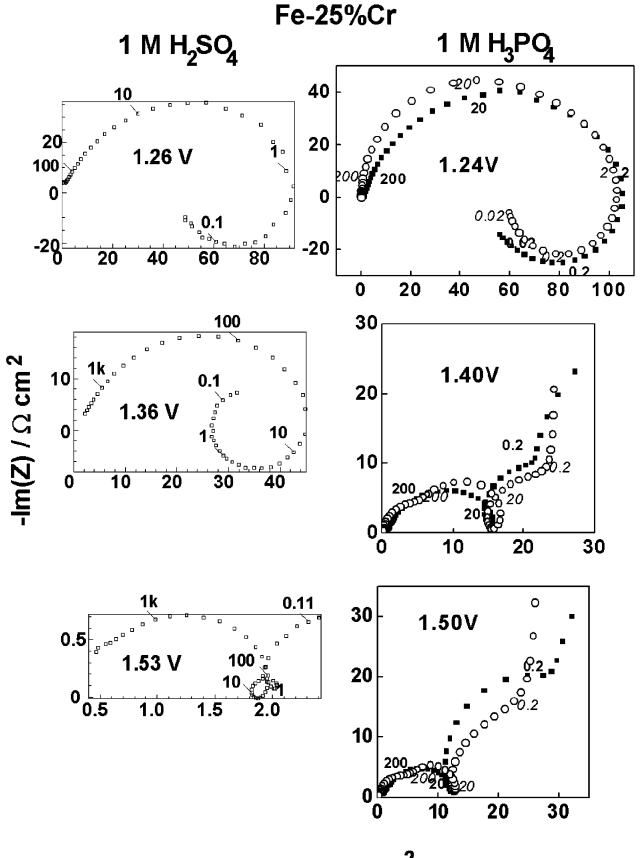

Figure 4. Impedance spectra of the Fe−25%Cr alloy in (left column) 1 M H_2SO_4 and (right column) 1 M H_3PO_4. Parameter is frequency in Hz. In the right column, full symbols are experimental values and empty symbols are best-fit calculation according to the proposed kinetic model.

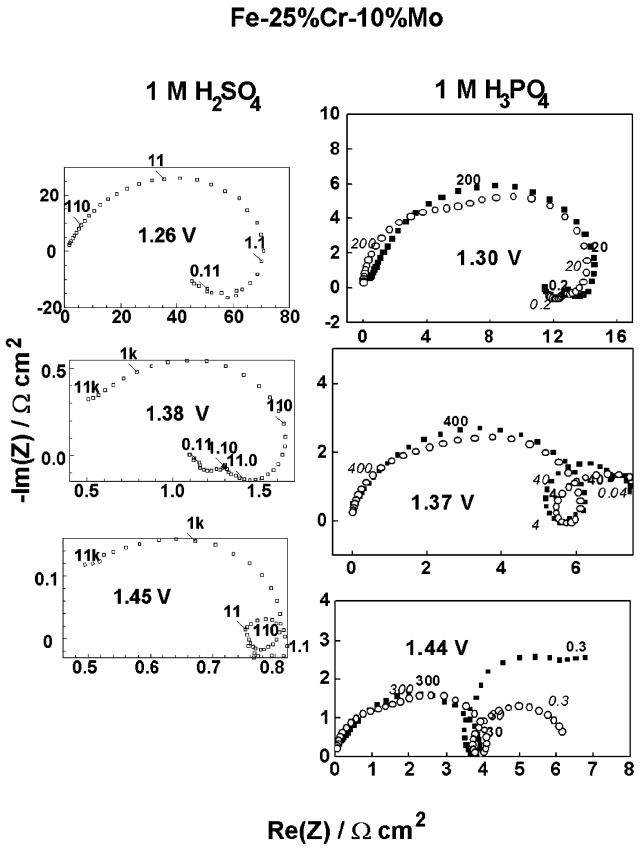

Figure 5. Impedance spectra of the Fe−25%Cr−10%Mo alloy in (left column) 1 M H_2SO_4 and (right column) 1 M H_3PO_4. Parameter is frequency in Hz. In the right column, full symbols are experimental values and empty symbols are best-fit calculation according to the proposed kinetic model.

in 1 M H_3PO_4 (cf. last spectra in the left and right columns of Figure 4). This observation can be interpreted once again in terms of a stabilization of the secondary passive state in phosphoric acid solution in comparison to 1 M H_2SO_4.

As commented already earlier,[14] the shape of the spectra measured for the Fe−25%Cr−10%Mo alloy in 1 M H_2SO_4 when compared to those for the Fe−25%Cr alloy (Figures 4 and 5) suggests a large predominance of the transpassive dissolution processes over secondary passivation for the Mo-containing alloy (evidenced as a predominantly pseudoinductive character of the impedance in the low-frequency region, left column of Figure 5). The transpassive dissolution reactions seem to be favored over the secondary passivation for Fe−25%Cr−10%Mo also in the 1 M H_3PO_4 solution (cf. the right columns of Figures 4 and 5). However, at the highest potentials (above 1.40 V), the low-frequency capacitive loop seems to dominate the impedance response of the Mo-containing alloy in phosphoric acid (cf. last spectra of the left and right columns of Figures 4 and 5). Accordingly, the magnitude of the low-frequency impedance for Fe−25%Cr−10%Mo in this potential region is significantly higher in 1 M H_3PO_4 than in 1 M H_2SO_4.

In contrast, the magnitude of the impedance for pure Cr in 1 M H_3PO_4 is smaller than that in 1 M H_2SO_4, the shapes of the spectra being practically identical (Figure 6). This means that the dissolution rate of Cr in the transpassive state is higher in phosphoric acid solution, the mechanism of the process remaining the same as that in sulfuric acid solution.

3.2. Nickel and Nickel-Based Alloys. *3.2.1. Voltammetric Measurements.* Figure 7 summarizes the voltammetric behavior

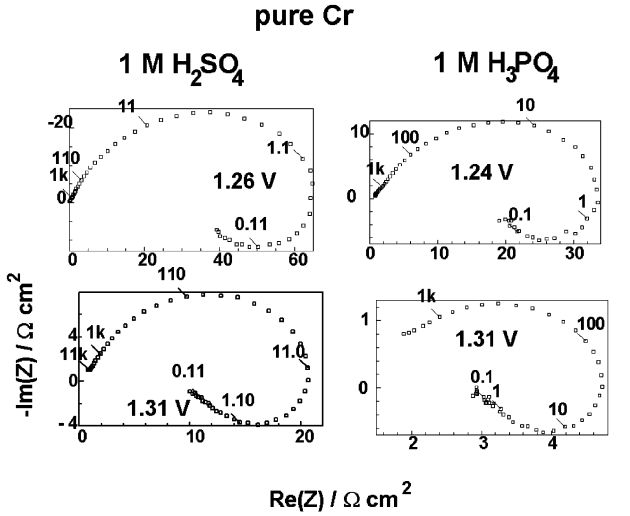

Figure 6. Impedance spectra of pure Cr in (left column) 1 M H_2SO_4 and (right column) 1 M H_3PO_4. Parameter is frequency in Hz.

of Ni and the studied nickel−chromium alloys during transpassive dissolution in 1 M H_2SO_4 (a) and H_3PO_4 (b). The transpassive dissolution currents of pure Ni in 1 M H_3PO_4 are significantly smaller than those in 1 M H_2SO_4, indicating that the interaction between phosphate and Ni(II) at the film/solution interface is considerably weaker than the same type of interaction between Ni(II) and sulfate. This kind of interaction has been considered to be one of the driving forces for the transpassivity of Ni in sulfate solutions.[17] Furthermore, secondary passivity (identified with the current plateau in 1 M H_3PO_4

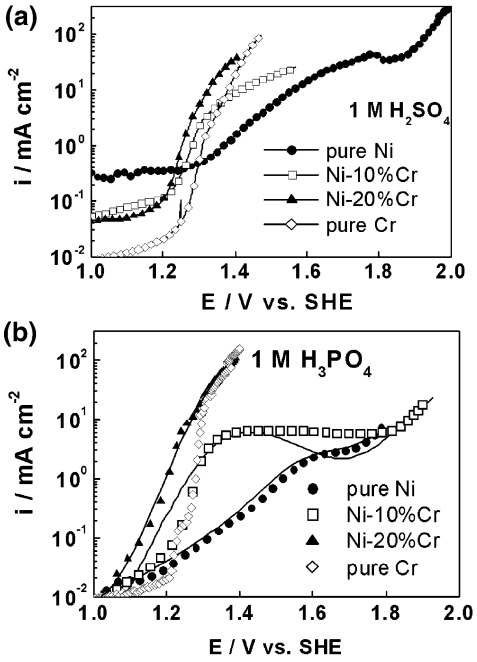

Figure 7. Current vs potential curves for pure Ni, pure Cr, and the studied Ni−Cr alloys in (a) 1 M H_2SO_4 and (b) 1 M H_3PO_4. Sweep rate = 1 mV s^{-1}; rotation rate = 600 rpm; points = experimental values; solid lines = best-fit calculation according to the proposed kinetic model.

as compared to the current maximum in 1 M H_2SO_4) is reached at a ca. 100 mV lower potential and correspondingly ca. 1 order of magnitude lower current density in phosphoric acid than in 1 M H_2SO_4 (Figure 7). This may mean that the phosphate anion has a certain stabilizing action on the intermediate species causing secondary passivation (which has been proposed in the literature to be a Ni(III) species[17]).

In a certain analogy to the results for the ferrous alloys (cf. Figure 1), the currents in the transpassive dissolution region (1.2−1.3 V) for the Ni−Cr alloys are very close to each other in both solutions (Figure 7). A noteworthy result reported also earlier in 1 M H_2SO_4[19] is that the transpassive dissolution rate of the Ni−20%Cr alloy is higher than that of pure Cr in 1 M H_3PO_4 (Figure 7). This has been connected to the higher ionic and electronic conductivity of the passive film on Ni−Cr alloys when compared to that on pure Cr.[20] In the secondary passivation region, however, the current exhibits a shallow maximum for Ni−10%Cr in 1 M H_3PO_4, whereas in 1 M H_2SO_4 only a decrease in slope is observed (Figure 7). This points to an increased efficiency of the secondary passivation in the phosphoric acid solution. Practically no such effect is observed for Ni−20%Cr, for which no significant difference in behavior between the phosphoric and sulfuric acid solution was noticed (Figure 7). This fact may be attributed to the increased effect of Cr on the processes in the transpassive region (as mentioned above, pure Cr dissolves transpassively at a faster rate in phosphoric than in sulfuric acid solution, Figure 6).

3.2.2. Impedance Spectroscopic Measurements. Figure 8 compares the impedance spectra of pure Ni in the transpassive region measured in 1 M H_2SO_4 (left column) and 1 M H_3PO_4 (right column). The data in 1 M H_2SO_4 are completely analogous to those reported by Keddam et al.[17] The impedance spectra comprise a high-frequency capacitive loop mainly due to the charge transfer at the film/solution interface[17] and a low-frequency combination of a capacitive and inductive loop situated either in the I and IV quadrant or circling the origin through all the four quadrants.[17,21] This indicates a second-order

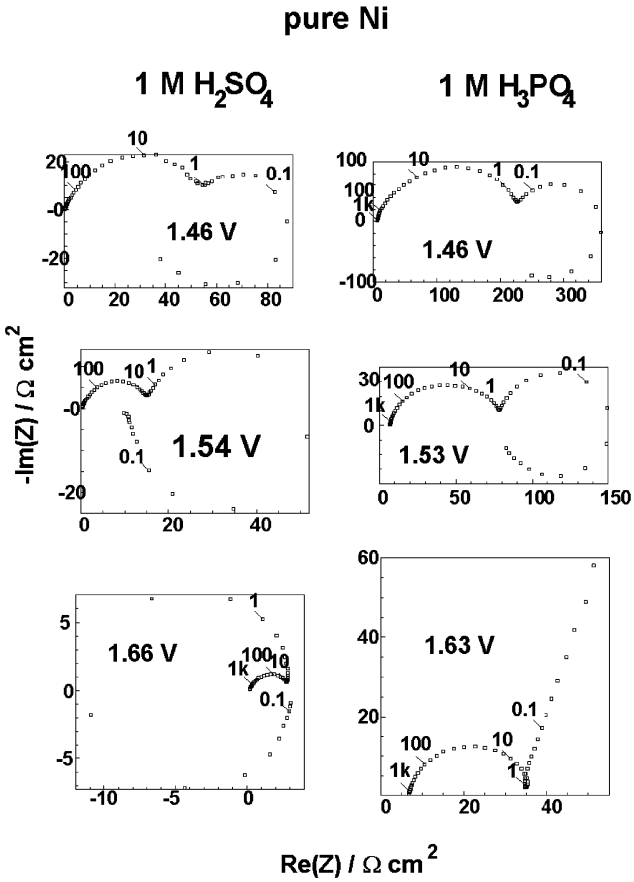

Figure 8. Impedance spectra of pure Ni in (left column) 1 M H_2SO_4 and (right column) 1 M H_3PO_4. Parameter is frequency in Hz.

dynamic behavior of the system and can be understood in terms of a competition of the transpassive dissolution and secondary passivation over the electrode surface.[17,21] The impedance magnitude at low frequencies in the 1 M H_3PO_4 solution is considerably higher than that in 1 M H_2SO_4 in accordance with the higher currents in the sulfuric acid medium (Figure 7). This fact indicates a much weaker interaction between the Ni(II) film and phosphate anion than that between the same film and sulfate and clearly demonstrates the role of the solution anion in the transpassive dissolution process.

The impedance spectra of Ni in phosphoric acid at the beginning of the secondary passivation region (above 1.60 V) indicated the formation of a secondary passive film (a low-frequency capacitive time constant with high resistance values, Figure 8) at difference to those in sulfuric acid, which still exhibited second-order dynamic behavior in the same potential range (up to 1.75 V). This observation points to a stabilization of the intermediate species causing secondary passivation by phosphate.

The spectra of the Ni−10%Cr alloy in the transpassive dissolution region (at 1.24 V, Figure 9) are qualitatively identical in both solutions, the impedance magnitude at low frequencies being slightly smaller in 1 M H_2SO_4. Thus the effect of the solution anion is small in this region, in accordance to the results for the ferrous alloys discussed previously (section 3.1.2.). However, the secondary passivation features (detected as a low-frequency capacitive loop) are observed at lower potentials in the 1 M H_3PO_4 solution (1.33 V) than in 1 M H_2SO_4 (1.37 V). Moreover, a further capacitive loop at lowest frequencies becomes quite prominent in the plateau region in 1 M H_3PO_4 (1.52 V, cf. Figures 7 and 9), whereas no reliable spectra could

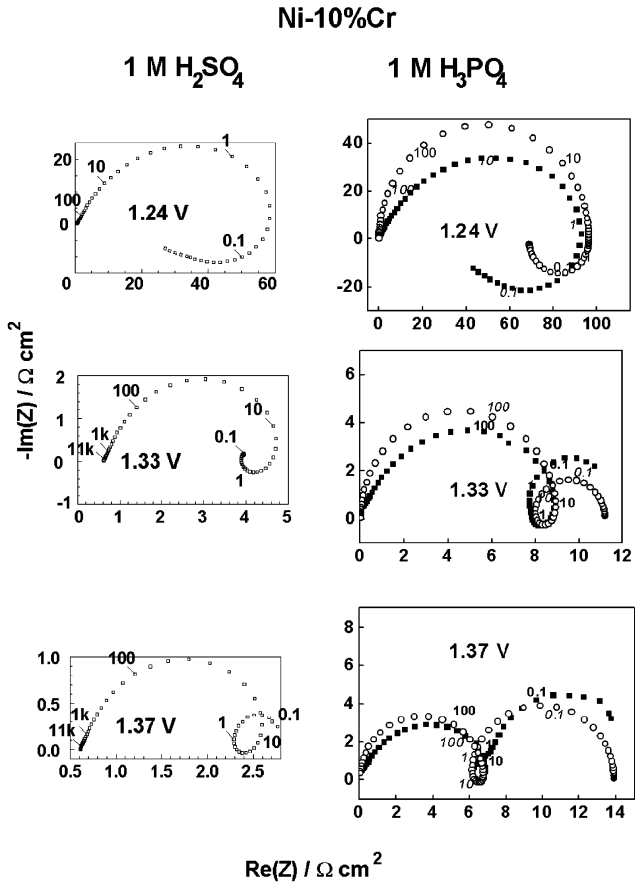

Figure 9. Impedance spectra of the Ni−10%Cr alloy in (left column) 1 M H_2SO_4 and (right column) 1 M H_3PO_4. Parameter is frequency in Hz. In the right column, full symbols are experimental values and empty symbols are best-fit calculation according to the proposed kinetic model.

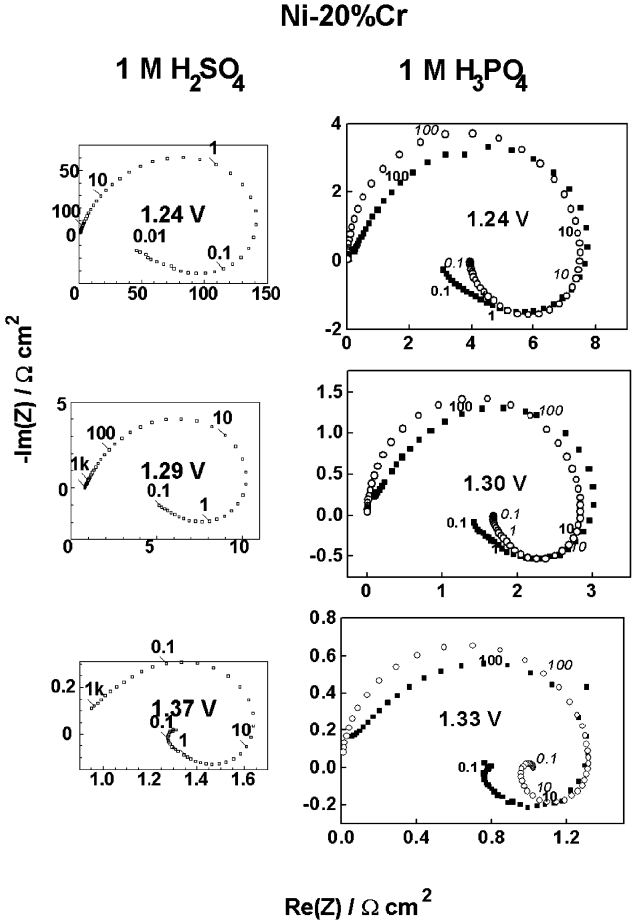

Figure 10. Impedance spectra of the Ni−20%Cr alloy in (left column) 1 M H_2SO_4 and (right column) 1 M H_3PO_4. Parameter is frequency in Hz. In the right column, full symbols are experimental values and empty symbols are best-fit calculation according to the proposed kinetic model.

be measured at such high potentials in 1 M H_2SO_4 because of the very high currents. The impedance spectra for Ni−10%Cr in the plateau region in 1 M H_3PO_4 bear some similarity to those for pure Ni (cf. right columns of Figures 8 and 9). Thus it can be tentatively suggested that the secondary passivation reaction via formation of a Ni(III)-based film stabilized by phosphate is responsible for the observed features also on the Ni−10%Cr alloy.

The impedance spectra of Ni−20%Cr alloy comprise only inductive loops in the low-frequency range, indicating that the tendency of this alloy to secondary passivation is very small in both studied media (Figure 10). Moreover, in analogy to pure Cr (cf. Figures 6 and 10), the impedance magnitude at low frequencies in the transpassive dissolution region (1.2−1.3 V) is smaller in phosphate solution than in 1 M H_2SO_4, which indicates that the rate of the transpassive dissolution of Cr from this alloy is higher in the phosphate medium. At higher potentials (above 1.3 V), there is some indication of the opposite trend (the impedance magnitude becomes smaller in 1 M H_2SO_4), but the very high currents preclude the performance of reliable impedance measurements in this potential range.

4. Reaction Model

4.1. Physicochemical Picture of a Transpassively Dissolving Metal or Alloy. A simplified scheme of the processes during transpassive dissolution of a hypothetical alloy containing Cr as the main alloying element is presented in Figure 11. The chemistry of the point defect model (PDM)[7] is employed in describing the reactions taking place at the interfaces, metal/film and film/solution, and a Kröger−Vink notation is used for the point defect chemistry.

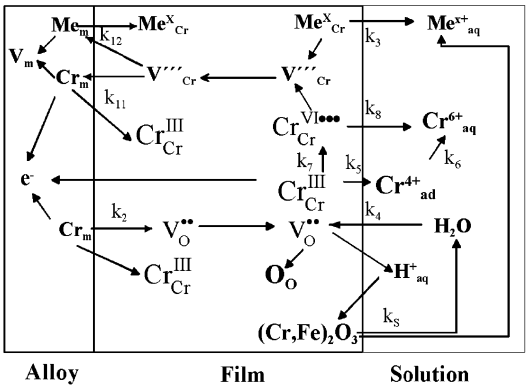

Figure 11. A general model of the transpassive dissolution of Cr-containing alloys. For the explanation of symbols, see Nomenclature.

4.1.1. Film Growth Process. The transpassive film is proposed to be a mixed oxide consisting essentially of Cr_2O_3 with some $Me^X \equiv Fe^{III}$, Ni^{II}, or $Mo^{V,VI}$ incorporated in it. The presence of a continuous barrier-like film at transpassive potentials was demonstrated in situ by ellipsometry,[22] modulated reflection spectroscopy,[23] and resistance measurements.[14,19,20]

At the metal/film interface, creation of normal Cr positions and generation of anion vacancies takes place (reaction step k_2 in Figure 11). The anion vacancies are transported through the

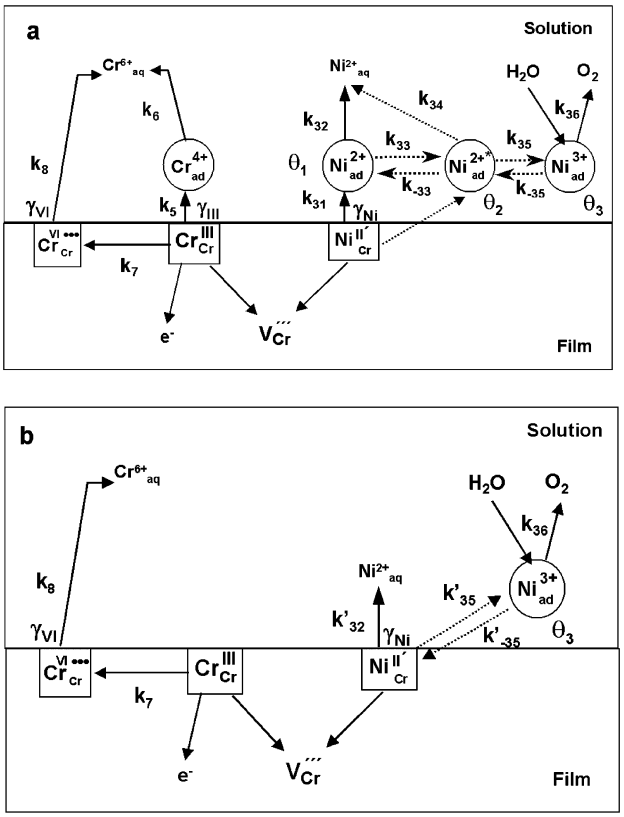

Figure 12. A scheme of the processes at the film/solution interface during transpassive dissolution of Ni−Cr alloys: (a) general scheme; (b) simplified scheme used to derive a quantitative model. For the explanation of symbols, see Nomenclature.

film via field-assisted migration and are annihilated at the film/solution interface to create normal oxygen positions in the oxide (reaction step k_4 in Figure 11). The oxide growth has to be balanced by its chemical dissolution (reaction step k_S in Figure 11) to achieve a steady-state thickness at a given potential.

4.1.2. Transpassive Dissolution of Cr. Two paths of transpassive dissolution of pure Cr have been proposed earlier by one of us.[9] One of the possible paths is a two-step reaction with an adsorbed intermediate (reaction sequence k_5-k_6 in Figure 11). This takes place at the Cr(III) positions in the outermost cation layer occupying a surface fraction γ_{III}. Another path for the transpassive dissolution proceeds via the oxidation of Cr(III) in the outermost layer of the film to Cr(VI) in a solid-state reaction, followed by a dissolution step leaving a chromium vacancy in the film (reaction sequence k_7-k_8 in Figure 11). The Cr cation vacancies created by the two sequences of reactions k_5-k_6 and k_7-k_8 are transported through the film and are consumed at the metal/film interface via the k_{11} reaction.

4.1.3. Dissolution of Other Metallic Constituents. Isovalent dissolution of Fe(III) substituted in Cr(III) positions in the oxide is expected to proceed on ferrous alloys at transpassive potentials via the simultaneous generation of cation vacancies[6,13,14] (reaction step k_3, Figure 11). The vacancies created by this process are consumed by the reaction step k_{12} analogous to k_{11} (Figure 11).

The transpassive dissolution of Ni is assumed to follow the mechanism proposed by Keddam et al.[17] as shown in Figure 12a. It is worthwhile to note that the role of the high-field migration of ions through the passive film in transpassive dissolution has been recognized by these authors as well (see ref 17, p 2564).

The steps characterized by rate constants k_{34} and k_{36} (Figure 12a) are autocatalytic in the sense that their rates do not depend on the coverages θ_2 and θ_3, respectively.[17] The cation vacancies generated by the reaction steps k_{31} and k_{34} (Figure 12a) are consumed at the metal/film interface in a reaction step analogous to k_{11} and k_{12}.

4.2. Main Assumptions of the Model. To transform the above physicochemical picture to a quantitative model, the following assumptions are made: (1) In accordance with the PDM,[5,7] the applied potential is distributed as potential drop in the bulk film and corresponding interfacial potential drops

$$E = \phi_{M/F} + \phi_{film} + \phi_{F/S} \tag{1}$$

where

$$\phi_{F/S} = \alpha E + \phi^0_{F/S} \tag{2}$$

$$\phi_{film} = \mathbf{E}L \tag{3}$$

$$\phi_{M/F} = (1-\alpha)E - \mathbf{E}L - \phi^0_{F/S} \tag{4}$$

E is the field strength in the film and α is the polarizability of the film/solution interface. For a detailed definition of all of the symbols used in the paper, the reader is referred to the Nomenclature section. (2) At the steady state, film thickness is assumed to be proportional to the applied potential[5,7]

$$L = (1-\alpha)E/(\mathbf{E} + L_{E=0}) \tag{5}$$

(3) From eqs 4 and 5, it follows that in the steady state $\phi_{M/F}$ is independent of the applied potential. We make a step further, assuming that this is true also in the transient regime. It follows that the reactions at the metal/film interface are not considered to be rate-limiting. Their rates are adjusted by the transport of point defects through the film. (4) The film growth process is limited by transport of oxygen vacancies. According to the surface charge approach (SCA) proposed earlier by one of us,[24] oxygen vacancies are transported via a high-field migration accelerated in the transient regime by a negative charge of cation vacancies at the film/solution interface. (5) In accordance to the PDM,[5,7] it is assumed that the field in the film is constant and buffered by electronic processes such as band-to-band tunneling analogous to polaron hopping. (6) Transpassive dissolution is limited by the reactions at the film/solution interface. In other words, the transport rate of cation vacancies in the film is assumed to be adjusted by the rate of their creation at the outer interface. The concentration of cation vacancies in the outermost cation layer is assumed to be negligble compared to the concentrations of normal cation positions in the film. (7) The rate constants of all of the reactions at the film/solution interface are assumed to depend exponentially on the potential drop at that interface, that is, $k_i = k_i^0 \exp(b_i E)$, $i = 3, ..., 8$, where k_i^0 is the value of the rate constant at the onset of transpassivity and $b_i = \alpha\alpha_i F/(RT)$, α_i being a transfer coefficient. An exponential dependence on potential is assumed to be valid also for ion-transfer reactions.[25] (8) No transport limitations for any species in the bulk electrolyte or in any kind of secondary (deposited or hydrated) layer are taken into account by the model.

4.3. Main Equations. *4.3.1. Ferrous Alloys.* In analogy to previous work in sulfate solutions,[13,14] it is assumed that the reaction of transpassive dissolution of Cr follows the reaction sequence k_5-k_6, that is, is a surface process as demonstrated also for pure Cr.[9,26] In other words, it is assumed that the

concentration of Cr(VI) in the outermost cation layer is negligible. This is thought to be physically reasonable in view of the fact that the film on Fe−Cr alloys at high potentials in the passive region is supposed to contain almost exclusively Cr(III) and Fe(III) cations, that is, the concentration of heterovalent defects is considered to be small. Such a view is in accordance with the relatively low electronic conductivity of the passive film as reported earlier by one of us.[20,27] The dissolution of Mo as Mo(VI) from the film is not considered as a separate reaction path for Fe−Cr−Mo alloys. Alternatively, Mo is assumed to substitute for Cr in the outermost cation layer or as nonstoichiometric molybdate species in the reaction layer at the solution side, accelerating the transpassive dissolution of Cr.[14,27]

4.3.1.1. Steady-State Current. For ferrous alloys, the steady-state current density at the film/solution interface in the transpassive state is given by

$$i_{ss} = F\{3k_3\gamma_{Fe_{ss}} + 3k_6\theta_{Cr_{ss}} + {}^4/_3k_4\} \tag{6}$$

where

$$\begin{aligned}\theta_{Cr_{ss}} &= k_3k_5x_{Cr}/[k_5k_6x_{Fe} + k_3x_{Cr}(k_5 + k_6)]\\ \gamma_{Fe_{ss}} &= k_5k_6x_{Fe}/[k_5k_6x_{Fe} + k_3x_{Cr}(k_5 + k_6)]\end{aligned} \tag{7}$$

The coefficient of $^4/_3$ in the last term at the right-hand side of eq 7 is derived from the oxygen/metal ratio in the oxide multiplied by the charge over an oxygen vacancy. Further, at steady state, the continuity equation imposes

$$k_4 = [D_Oc_O(L)/(2a)]\exp(2Fa\mathbf{E}/(LRT)) \tag{8}$$

because the steady-state rate of consumption of oxygen vacancies at the film/solution interface must adjust to the steady-state rate of oxygen vacancy transport in the film. For additional details on the derivation, the reader is referred to previous publications.[13,14]

4.3.1.2. Small Amplitude ac Response. For ferrous alloys, the overall impedance is the sum of the impedances of the film and of the film/solution interface:

$$Z = Z_f + Z_{F/S} = d\phi_f/di + d\phi_{F/S}/di \tag{9}$$

The impedance of the film is given by the equation derived in the surface charge approach[20,24]

$$Z_f = \{i_{SS}(2Fa/(RT))\{(1-\alpha) + i_{SS}S/[j\omega + i_{SS}S]\}/L + j\omega C_f\}^{-1} \tag{10}$$

where S is the capture cross section for a current carrier and C_f is the capacitance of the oxide film or the space charge layer. The impedance of the film/solution interface is given by[13,14]

$$Z_{F/S} = [R_t^{-1} + F\{(3k_3 - k_5)\,d\gamma_{Fe}/dE + (2k_6 - k_5)\,d\theta_{Cr}/dE\} + j\omega C_{F/S}]^{-1} \tag{11}$$

where

$$\begin{aligned}R_t^{-1} &= \alpha F\{3b_3k_3\gamma_{Fe_{ss}} + {}^4/_3b_4k_4 + (b_5 + 2b_6)k_6\theta_{Cr_{ss}}\}\\ d\theta_{Cr}/dE &= (X_2Z_1 - k_5X_1)/(Z_1Z_2 + k_5k_6x_{Fe})\\ d\gamma_{Fe}/dE &= (X_1Z_2 + k_6x_{Fe}X_1)/(Z_1Z_2 + k_5k_6x_{Fe})\\ X_1 &= \alpha(b_6k_6x_{Fe}\theta_{Cr_{ss}} - b_3k_3x_{Cr}\gamma_{Fe_{ss}})\\ X_2 &= \alpha(b_5 - b_6)k_6\theta_{Cr_{ss}}\\ Z_1 &= j\omega\beta + k_3x_{Cr}\\ Z_2 &= j\omega\beta + k_5 + k_6\end{aligned} \tag{12}$$

and $C_{F/S}$ is the double layer capacitance at the film/solution interface.

4.3.2. Nickel-Based Alloys. For Ni−Cr alloys, film growth is considered to be a slow process in parallel to transpassive dissolution and is accordingly neglected.[19,28] Further, the transpassive dissolution of Cr is supposed to proceed via the reaction path k_7−k_8, that is, some concentration of $Cr_{Cr}^{VI\bullet\bullet\bullet}$ is assumed to be maintained in the outermost cation layer.[19] Cr(VI) has been detected in the passive films formed on Ni−20%Cr at high potentials in sulfuric acid solution.[29] The presence of Cr(VI) is considered physically logical in view of the presence of heterovalent substitutional defects such as $Ni_{Cr}^{II'}$ in the oxide film (Figure 12), increasing the overall degree of nonstoichiometry. This fact is in accordance with the considerably higher electronic conductivity of the passive film formed on Ni−Cr alloys in comparison to Fe−Cr alloys.[20]

Next, based on the data from the Results section, the increased importance of secondary passivation in phosphate solutions can be interpreted by the enhanced role of the reaction steps involving Ni_{ad}^{3+} intermediate over those involving Ni_{ad}^{2+} and $Ni*_{ad}^{2+}$ species in the reaction sequence (Figure 12a). In other words, it appears reasonable to neglect the surface covered with Ni_{ad}^{2+} and $Ni*_{ad}^{2+}$ and depict the reaction sequence of transpassive dissolution of Ni in a simplified form, as shown in Figure 12b.

In kinetic terms, this means that the step k_{31} is considered as fast in comparison to k_{32}, k_{33}/k_{-33} is assumed to be in equilibrium, and k_{34} is always smaller than k_{35}. It has been proposed in ref 17 for pure Ni and further adopted in ref 28 for nickel-based alloys that the $Ni*_{ad}^{2+}$ is stabilized by sulfate. Alternatively, we assume here that $Ni*_{ad}^{2+}$ is destabilized and Ni_{ad}^{3+} is stabilized by phosphate. The validity of such an assumption will be checked a posteriori by the comparison of the model predictions with experimental data.

4.3.2.1. Steady-State Current. According to the above assumptions, the steady-state current for nickel-based alloys in phosphate solution is given by

$$i_{ss} = F[(2k'_{32} + k'_{35})\gamma_{Ni_{ss}} + 3k_7\gamma_{III_{ss}} + 2k_{36}\theta_{3_{ss}}] \tag{13}$$

where

$$\begin{aligned}\gamma_{Ni_{ss}} &= k'_{-35}k_7k_8(1 - x_{III})/D\\ \gamma_{III_{ss}} &= k'_{32}k'_{-35}k_8x_{III}/D\\ \theta_{3_{ss}} &= k'_{35}k_7k_8(1 - x_{III})/D\\ D &= x_{III}k'_{32}k'_{-35}(k_7 + k_8) + (1 - x_{III})k_7k_8(k'_{35} + k'_{-35})\end{aligned} \tag{14}$$

4.3.2.2. Small Amplitude ac Response. As mentioned above, the overall impedance is assumed to coincide with the impedance of the film/solution interface. This impedance has the form

$$Z_{F/S}^{-1} = R_t^{-1} + F[(2k'_{32} + k'_{35})(d\gamma_{Ni}/dE) + 3k_7(d\gamma_{III}/dE) + 2k_{36}(d\theta_3/dE)] + j\omega C_{F/S} \quad (15)$$

where

$$R_t^{-1} = F[(2b'_{32}k'_{32} + b'_{35}k'_{35})\gamma_{Ni_{ss}} + 3b_7k_7\gamma_{III_{ss}} + 2b_{36}k_{36}\theta_{3_{ss}}]$$

$$d\gamma_{Ni}/dE = [Z_3k_8(1 - x_{III})(k_7X_2 + X_4Z_2) + (k'_{-35} - X_1)Z_3(Z_2Z_4 - k_7k_8x_{III})]/Z_D$$

$$d\gamma_{III}/dE = [X_2Z_4 + k_8x_{III}X_4 + k'_{32}x_{III}Z_4(d\gamma_{Ni}/dE)]/(Z_2Z_4 - k_7k_8x_{III})$$

$$d\theta_3/dE = [X_3 + k'_{35}(d\gamma_{Ni}/dE)]/Z_3$$

$$X_1 = b_8k_7\gamma_{III_{ss}}(1 - x_{III}) - (b'_{32}k'_{32}x_{III} + b'_{35}k'_{35})\gamma_{Ni_{ss}} + b'_{-35}k'_{-35}\theta_{3_{ss}} \quad (16)$$

$$X_2 = b'_{32}k'_{32}x_{III}\gamma_{Ni_{ss}} + (b_8x_{III} - b_7)\gamma_{III_{ss}}$$

$$X_3 = (b'_{35} - b'_{-35})k'_{-35}\theta_{3_{ss}}$$

$$X_4 = (b_7 - b_8)\gamma_{III_{ss}}$$

$$Z_1 = j\omega\beta + k'_{35} + k'_{32}x_{III}$$

$$Z_2 = j\omega\beta + k_7$$

$$Z_3 = j\omega\beta + k'_{-35}$$

$$Z_4 = j\omega\beta + k_8$$

$$Z_D = (Z_2Z_4 - k_7k_8x_{III})(Z_3Z_1 - k'_{35}k'_{-35}) - k'_{32}k_7k_8x_{III}(1 - x_{III})Z_3$$

5. Comparison of the Model with Experimental Data

A nonlinear least-squares routine was used to fit the model equations simultaneously to the real and imaginary part of the measured impedance for a specific alloy at several potentials and to the corresponding current vs potential curve. Statistical weighting was used for the experimental data set, and the errors of parameter estimation were multiplied by the square root of the reduced χ^2 value resulting from the fit. Despite the relatively large number of parameters, this resulted in a sufficient number of degrees of freedom in the system to obtain statistically reliable values of the kinetic parameters. The goodness of fit and the physical significance of the kinetic parameters are discussed below.

5.1. Ferrous Alloys. Figure 1b shows a comparison of the current vs potential curves as calculated from the model (solid lines) with the experimental data for the four ferrous alloys studied. The corresponding fitting results for the alloys in 1 M H_2SO_4 have been already published.[13,14] The main features of the experimental data are reproduced by the model, namely, the relatively small differences among materials in the potential range 1.1−1.3 V and the subsequent divergence of the curves in the secondary passivation region (1.3−1.6 V). The calculated current magnitude agrees plausibly with the experimental data as well. The main discrepancy between the model and the experiment is that no current plateau is predicted by the model, especially for the alloys containing 25%Cr. Instead, the current continues to increase in the secondary passivation region, albeit at a very low rate when compared to that in the transpassive dissolution region. This discrepancy may be because the current plateau is determined by the rate of formation/dissolution of some kind of secondary layer or to an acceptor mechanism involving direct interaction between dissolving Fe cations and the anion from the solution, as propsed, for example, by Matlosz et al. for electropolishing of ferritic steels in mixtures of concentrated phosphoric and sulfuric acids.[30] However, it has been judged unnecessary to further complicate our model without direct evidence for such processes.

The ability of the model to account for the experimental impedance response is illustrated in the right columns of Figures 2 (Fe−12%Cr), 3 (Fe−12%Cr−5%Mo), 4 (Fe−25%Cr), and 5 (Fe−25%Cr−10%Mo) (see Results section). For the alloys containing 12%Cr, the agreement between the model calculations and the experimental data is very good in the whole studied potential interval (1.2−1.6 V, Figures 2 and 3). Both the magnitude and the frequency response of the impedance are predicted with good accuracy. The quality of the fit is somewhat worse at the highest frequencies probably because a pure interfacial capacitance was used instead of the more commonly employed constant phase element (CPE). However, because the exact physical meaning of the CPE on a real corroding surface is still a matter of debate, we preferred not to include it in our modeling.

For the alloys containing 25%Cr, the agreement between the calculated and experimental data is very good in the potential interval 1.2−1.4 V (Figures 4 and 5). At higher potentials in the secondary passivation region, however, the agreement is somewhat worse is in accordance with the discrepancy between the calculated and experimental current vs potential curves for these materials in the same potential interval (Figure 1b). It seems that an extra time constant detected in the experimental data is not predicted accurately by the model. Such a time constant connected with a homogeneous or heterogeneous chemical reaction of interaction between dissolving Fe and a solution anion has been included, for example, in the model proposed by Matlosz et al.[30] Also in this case, we decided that to include such a step in our model will be speculative and will unnessecarily complicate the calculation procedure without adding value to our understanding of the transpassive dissolution process.

Table 1 collects the kinetic parameters determined by the best-fit calculation for the studied ferrous alloys. The following points are worth emphasizing: (1) In analogy to the parameters previously reported for 1 M H_2SO_4,[13,14] the rate constant and especially the Tafel coefficient of the reaction of Fe dissolution (k_3 step) increase with increasing Cr content in the alloy. Such increase is in agreement with previous data for Fe−Cr alloys reported by Heusler.[31] The addition of Mo to the alloys leads to a further increase of that reaction step (Table 1). However, this increase in the case of Fe−25%Cr−10%Mo is not as pronounced in 1 M H_3PO_4 as in a sulfuric acid solution.[14] Such a result is in general agreement with the smaller effect of Mo addition on the transpassive dissolution rate in 1 M H_3PO_4, as shown in the Results section. (2) The parameters characterizing the transport through the transpassive film (field strength, half-jump distance, and capture cross section) remain essentially independent of the alloy composition, indicating that the oxide films on different alloys are to a great extent similar. The polarizability of the film/solution interface is higher for the alloys with higher Cr content, also in accordance with the data

TABLE 1: Kinetic Parameters of the Transpassive Dissolution Process for Ferrous Alloys Determined by a Best-Fit Calculation from the Data in 1 M H_3PO_4

parameter	Fe−12%Cr	Fe−12%Cr−5%Mo	Fe−25%Cr	Fe−25%Cr−10%Mo
k_3, mol cm^{-2} s^{-1}	4×10^{-10}	7×10^{-10}	5×10^{-10}	9×10^{-10}
b_3, V^{-1}	1.5	3	12	22
k_4, mol cm^{-2} s^{-1}	5×10^{-11}	4.5×10^{-11}	2.6×10^{-11}	6×10^{-11}
b_4, V^{-1}	20	22	22	23
k_5, mol cm^{-2} s^{-1}	1.7×10^{-10}	1.9×10^{-10}	1.9×10^{-10}	1.7×10^{-10}
b_5, V^{-1}	31	33	36	34
k_6, mol cm^{-2} s^{-1}	7.5×10^{-7}	7.5×10^{-7}	3×10^{-7}	2×10^{-7}
b_6, V^{-1}	4.5	6	6	6
x_{Fe}	0.35	0.35	0.25	0.2
β, mol cm^{-2}	0.5×10^{-8}	1×10^{-8}	1×10^{-8}	1×10^{-8}
α	0.36	0.35	0.45	0.59
$C_{F/S}$, μF cm^{-2}	160	240	260	300
E, MV cm^{-1}	3.3	4.0	3.4	3.0
a, nm	0.7	0.6	0.6	0.6
ϵ	42	50	33	52
S, mC^{-1} cm^2	3.0	3.0	2.0	1.6

in 1 M H_2SO_4, but the differences between the alloys containing 12% and 25% Cr are smaller in 1 M H_3PO_4 than in the sulfuric acid solution.[13,14] (3) The rate constants of both steps in the transpassive dissolution process (k_5 and k_6) are higher in phosphoric acid solution than in 1 M H_2SO_4. This is in accordance with the higher transpassive dissolution rate of pure Cr in 1 M H_3PO_4 when compared to that in 1 M H_2SO_4 (Figure 6). On the other hand, the Tafel coefficients for both reaction steps k_5 and k_6 are smaller in 1 M H_3PO_4 than in the sulfuric acid solution (Table 1 and refs 13 and 14).

5.2. Nickel-Based Alloys. Figure 7b shows a comparison of the current vs potential curves as calculated from the model (solid lines) with the experimental data for pure Ni and the two nickel-based alloys studied. It is noteworthy to mention that we simulated the data for pure Ni directly with the model proposed by Keddam et al. as described in ref 17 (cf. the reaction sequence depicted in Figure 12). The agreement between experiment and calculation is very good for pure Ni and Ni−20%Cr alloy, leaving somewhat to desire for Ni−10%Cr. However, the main features of the experimental data (the current maximum at ca. 1.35 V and the further increase in the current at potentials higher than 1.75 V) are reproduced by the model together with the magnitude of the current in the whole potential range studied. To predict more accurately the current vs potential curve for the Ni−10%Cr alloy, introduction of additional reaction steps has been found to be necessary. Preliminary trials with a model in which the intermediate species Ni_{ad}^{2+} and $Ni*_{ad}^{2+}$ are introduced were found to give better results for the current vs potential curve, but the increased number of parameters compromised the statistical validity of the calculation procedure. We therefore decided to use the relatively simple model proposed here to extract meaningful values of the kinetic parameters.

The ability of the model to account for the experimental impedance response is illustrated in the right columns of Figures 8 (pure Ni), 9 (Ni−10%Cr), and 10 (Ni−20%Cr). It can be concluded that both the impedance magnitude and frequency distribution are satisfactorily reproduced by the model. The agreement between calculated and experimental data is somewhat worse for the Ni−10%Cr alloy when compared to Ni−20%Cr. This fact is in accordance with the degree of reproduction of the voltammetric curve for the same alloy. However, as mentioned already above, we have found that increasing the number of parameters by introducing the intermediate species Ni_{ad}^{2+} and $Ni*_{ad}^{2+}$ leads to a loss of the statistical significance of the calculation. Thus the simpler model was employed also for the calculation of the parameters from the impedance spectra.

TABLE 2: Kinetic Parameters of the Transpassive Dissolution Process for Nickel-Based Alloys Determined by a Best-Fit Calculation from the Data in 1 M H_3PO_4[a]

parameter	pure Ni	Ni−10%Cr	Ni−20%Cr
k'^{0}_{32}, mol cm^{-2} s^{-1}	4×10^{-11}	2×10^{-9}	7×10^{-9}
b'_{32}, V^{-1}	8	6	10
k'^{0}_{35}, mol cm^{-2} s^{-1}	1.5×10^{-11}	2×10^{-14}	1.5×10^{-14}
b'_{35}, V^{-1}	10	10	7
k'^{0}_{-35}, mol cm^{-2} s^{-1}	7×10^{-9}	7×10^{-12}	7×10^{-12}
b'_{-35}, V^{-1}	−4.5	−6	−6
k^0_{36}, mol cm^{-2} s^{-1}	1.5×10^{-12}	5×10^{-13}	5×10^{-13}
b_{36}, V^{-1}	12.5	13	13
k^0_7, mol cm^{-2} s^{-1}		1×10^{-9}	7×10^{-9}
b_5, V^{-1}		18	17
k^0_8, mol cm^{-2} s^{-1}		2×10^{-11}	1×10^{-11}
b_8, V^{-1}		29	34
β, mol cm^{-2}	1×10^{-8}	2×10^{-8}	1×10^{-8}
$C_{F/S}$, μF cm^{-2}	100	100	120
x_{Ni}		0.35	0.2

[a] The corresponding parameters calculated from a best-fit of the model of Keddam et al.[17] to the data for pure Ni in 1 M H_3PO_4 are included for comparison.

Table 2 collects the kinetic parameters of transpassive dissolution of the nickel-based alloys as determined by the best-fit calculation. The values of the common kinetic parameters for pure Ni are also shown in the table for comparison. The following points are worth emphasizing: (1) Both the rate constant and the Tafel coefficient of the Ni dissolution as Ni(II) (k'_{32} step, Figure 12b) increase with increasing Cr content in the alloy. This points to some analogy with ferrous alloys regarding the accelerating effect of Cr on the dissolution of the main element. (2) The rate constant and the Tafel coefficient of the secondary passivation reaction (k'_{35} step, Figure 12b) are somewhat smaller for the Ni−20%Cr alloy than for Ni−10%Cr, demonstrating the decreasing efficiency of secondary passivation with increasing Cr content in the alloy. Indeed, the rate constant of this reaction for pure Ni is significantly higher (Table 2). (3) The rate constant and the Tafel coefficient of the oxygen evolution reaction (k_{36} step) on the alloys are close to those for pure Ni. This most probably means that the mechanism of oxygen evolution remains essentially unchanged, proceeding on the Ni(III) catalytic sites. (4) The rate constant of the solid-state oxidation step k_7 in the transpassive dissolution of Cr increases with increasing Cr content in the alloy, the values being practically the same as those calculated earlier for the same alloys in 1 M H_2SO_4.[19] The values of the Tafel coefficient of this step are also very close to those in 1 M H_2SO_4. On the other hand, the rate constant of the dissolution of Cr(VI) as chromate (k_8 step) is considerably higher in 1 M H_3PO_4 than in

1 M H_2SO_4, which seems to be in accordance to the fact that transpassive dissolution of pure Cr is faster in the phosphoric acid solution (see Figure 6).

6. Conclusions

The main aim of this work has been to generalize the kinetic model for transpassive dissolution to include the effects of solution anion on the individual reaction steps. For the purpose, experimental data on the transpassive dissolution of a range of ferrous- and nickel-based alloys in 1 M H_3PO_4 are compared with corresponding data in 1 M H_2SO_4 to gain a better insight in the influence of the solution anion on the processes in the transpassive state.

From the experimental data, it can be concluded that the nature of the solution anion has a significant influence on the dissolution reaction of the main element (Fe and Ni). Namely, the secondary passivation reaction is enhanced in 1 M H_3PO_4 in comparison to the sulfuric acid solution. On the other hand, the nature of the solution anion has a comparatively smaller effect on the transpassive dissolution reaction of Cr itself.

For ferrous alloys, it can be concluded that the model proposed earlier to account for the transpassive dissolution in sulfate solutions remains in general valid also in phosphoric acid solution. However, the increased tendency toward secondary passivation in phosphoric acid solution when compared to 1 M H_2SO_4 points to a change in the mechanism of dissolution of the main element, Fe, from the alloys. An additional reason for the enhancement of secondary passivation is the decrease of the accelerating effect of Mo on the transpassive dissolution of Cr in phosphoric acid solution in comparison to 1 M H_2SO_4.

For nickel-based alloys, a modification of the model proposed earlier for the transpassive state in 1 M H_2SO_4 was needed to reproduce the data obtained in 1 M H_3PO_4. This is most probably because the tendency of Ni to secondary passivation is much more pronounced in phosphoric acid than in sulfuric acid solution. Accordingly, an oxidation step of Ni(II) at the film/solution interface to an intermediate species, Ni(III), causing secondary passivation, has been added to the kinetic model for nickel-based alloys. Calculation results have shown that to reproduce the data for Ni−10%Cr in a fully quantitative way further intermediate species have to be introduced. However, the first attempts to further complicate the model have been found to have negative influence on the statistical validity of the calculation procedure. It is therefore clear that additional experimental data are needed to fully explore the possibilities of the model approach to reproduce the influence of the solution anion on the transpassive dissolution process.

Nomenclature

a = atomic jump distance, cm.

b_i = Tafel coefficients of the interfacial reactions ($i = 1-8$), V^{-1}.

$c_O(L)$ = concentration of oxygen vacancies at the metal/film interface, mol cm^{-3}.

C_f = high-frequency capacitance of the film, F cm^{-2}.

$C_{F/S}$ = capacitance of the cation vacancy accumulation layer, F cm^{-2}.

Cr_m = Cr atom in the metal phase.

Cr_{Cr}^{III} = chromium(III) in a chromium position in the anodic film.

$Cr_{Cr}^{VI\bullet\bullet\bullet}$ = chromium(VI) in a chromium position in the anodic film.

Cr_{ad}^{4+} = adsorbed Cr(IV) intermediate at the film/solution interface.

D_O = diffusion coefficient of oxygen vacancies, $cm^2\ s^{-1}$.

E = applied potential, V.

$\mathbf{E}$ = electric field strength, V cm^{-1}.

Fe_{Cr}^{III} = iron(III) in a chromium position in the anodic film.

i = current density, A cm^{-2}.

i_{ss} = steady-state current density, A cm^{-2}.

j = imaginary unit.

k_i = rate constants of the interfacial reactions ($i = 1-8$), mol $cm^{-2}\ s^{-1}$.

k_S = rate constant of the chemical dissolution of the film, mol $cm^{-2}\ s^{-1}$.

L = thickness of the anodic film, cm.

$L_{E=0}$ = thickness of the anodic film at $E = 0$, cm.

Me_m = metal atom (Me = Fe, Ni) in the metal phase.

$Ni_{Cr}^{II'}$ = nickel(II) in a chromium position in the anodic film.

Ni_{ad}^{2+} = nickel(II) intermediate adsorbed at the film/solution interface.

$Ni*_{ad}^{2+}$ = nickel(II) intermediate adsorbed at the film/solution interface.

Ni_{ad}^{3+} = nickel(III) intermediate adsorbed at the film/solution interface.

O_O = oxygen position in the anodic film.

R_t = charge-transfer resistance, $\Omega\ cm^2$.

$V_O^{\bullet\bullet}$ = oxygen vacancy in the anodic film.

V_{Cr}''' = chromium cation vacancy in the anodic film.

S = capture cross section for a positive defect, $cm^2\ C^{-1}$.

x_{Fe} = fraction of iron(III) positions in the film bulk.

x_{III} = fraction of chromium(III) positions in the film bulk.

x_{Ni} = fraction of nickel(II) positions in the film bulk.

Z_f = impedance of the anodic film, $\Omega\ cm^2$.

$Z_{F/S}$ = impedance of the film/solution interface, $\Omega\ cm^2$.

α = polarizability of the film/solution interface.

β = total number of cation positions in the outermost layer of the film, mol cm^{-2}.

γ_{Fe} = fraction of iron(III) positions in the outermost layer of the film.

γ_{III} = fraction of chromium(III) positions in the outermost layer of the film.

γ_{VI} = fraction of chromium(VI) positions in the outermost layer of the film.

γ_{Ni} = fraction of nickel(II) positions in the outermost layer of the film.

ϵ = dielectric constant of the film.

ϵ_0 = dielectric permittivity of vacuum.

$\phi_{M/F}$ = local potential drop at the metal/film interface, V.

$\phi_{F/S}$ = local potential drop at the film/solution interface, V.

θ_{Cr} = surface coverage of Cr_{ad}^{4+} intermediate.

θ_1 = surface coverage of Ni_{ad}^{2+} intermediate.

θ_2 = surface coverage of $Ni*_{ad}^{2+}$ intermediate.

θ_3 = surface coverage of Ni_{ad}^{3+} intermediate.

ω = angular frequency, rad s^{-1}.

References and Notes

(1) Wyllie, W. E., II; Duquette, D. J. *Corrosion* **1998**, *54*, 781.
(2) Wensley, A.; Dykstra, H. *Pulp Pap. Can.* **1997**, *98*, 40.
(3) Bellanger, G.; Rameau, J.-J. *Mater. Sci.* **1996**, *31*, 2097.
(4) Kawashima, A.; Asami, K.; Hashimoto, K. *Corros. Sci.* **1985**, *25*, 1103.
(5) Lin, L.; Chao, C.; Macdonald, D. D. *J. Electrochem. Soc.* **1981**, *128*, 1194.
(6) Betova, I.; Bojinov, M.; Kinnunen, P.; Pohjanne, P.; Saario, T. *Electrochim. Acta* **2002**, *47*, 3335.
(7) Macdonald, D. D. *J. Electrochem. Soc.* **1992**, *139*, 3434.

(8) Macdonald, D. D. In *2001 Joint International Meeting: The 200th Meeting of the Electrochemical Society and the 52nd Meeting of the International Society of Electrochemistry*, San Francisco, CA, Proceedings of the Electrochemical Society, Vol. 2001-2; The Electrochemical Society, Inc.: Pennington, NJ, 2001; Abstract No. 486.

(9) Bojinov, M.; Fabricius, G.; Laitinen, T.; Saario, T. *J. Electrochem. Soc.* **1998**, *145*, 2043.

(10) Kirchheim, R.; Heine, B.; Fischmeister, H.; Hofmann, S.; Knote, H.; Stolz, U. *Corros. Sci.* **1989**, *29*, 899.

(11) Ben-Haim, M.; Atzmony, U.; Shamir, N. *Corrosion* **1988**, *44*, 461.

(12) Atrens, A.; Baroux, B.; Mantel, M. *J. Electrochem. Soc.* **1997**, *144*, 3697.

(13) Bojinov, M.; Betova, I.; Fabricius, G.; Laitinen, T.; Raicheff, R.; Saario, T. *Corros. Sci.* **1999**, *41*, 1557.

(14) Bojinov, M.; Fabricius, G.; Laitinen, T.; Saario, T. *Electrochim. Acta* **1999**, *44*, 4331.

(15) Arlt, N.; Heimann, W.; Ladwein, T.; Michel, E. *Thyssen Edelstahl Tech. Ber.* **1991**, *17*, 16.

(16) Laycock, N. J.; Newman, R. C.; Stewart, J. *Corros. Sci.* **1995**, *37*, 1637.

(17) Keddam, M.; Takenouti, H.; Yu, N. *J. Electrochem. Soc.* **1985**, *132*, 2561.

(18) Bojinov, M.; Betova, I.; Raicheff, R. *J. Electroanal. Chem.* **1997**, *430*, 169.

(19) Bojinov, M.; Fabricius, G.; Kinnunen, P.; Laitinen, T.; Mäkelä, K.; Saario, T.; Sundholm, G. *Electrochim. Acta* **2000**, *45*, 2791.

(20) Bojinov, M.; Kinnunen, P.; Laitinen, T.; Mäkelä, K.; Saario, T. In *Corrosion and Corrosion Protection*; Sinclair, J., Kalman, E., Frankenthal, R., Plieth, W., Eds.; Proceedings of the Electrochemical Society, Vol. 2001-22; The Electrochemical Society, Inc., Pennington, NJ, 2001; p 26.

(21) Bojinov, M. *J. Electroanal. Chem.* **1996**, *405*, 15.

(22) Sugimoto, K.; Matsuda, S. *Mater. Sci. Eng.* **1980**, *42*, 181.

(23) Hara, N.; Sugimoto, K. *J. Electrochem. Soc.* **1979**, *126*, 1328.

(24) Bojinov, M. *Electrochim. Acta* **1997**, *42*, 3489.

(25) Heusler, K. E.; Stöckgen, U. In *Passivity and Its Breakdown*; Natishan, P., Isaacs, H.; Janik-Czachor, M., Macagno, V., Marcus, P., Seo, M., Eds.; Proceedings of The Electrochemical Society, Vol. 97-26; The Electrochemical Society, Inc.: Pennington, NJ, 1998; p 243.

(26) Schmuki, P.; Virtanen, S.; Davenport, A.; Vitus, C. *J. Electrochem. Soc.* **1996**, *143*, 3997.

(27) Bojinov, M.; Fabricius, G.; Laitinen, T.; Mäkelä, K.; Saario, T.; Sundholm, G. *Electrochim. Acta* **2001**, *46*, 1358.

(28) Betova, I.; Bojinov, M.; Kinnunen, P.; Laitinen, T.; Pohjanne, P.; Saario, T. *Electrochim. Acta* **2002**, *47*, 2093.

(29) Jabs, T.; Borthen, P.; Strehblow, H.-H. *J. Electrochem. Soc.* **1997**, *144*, 1231.

(30) Matlosz, M.; Magaino, S.; Landolt, D. *J. Electrochem. Soc.* **1994**, *141*, 410.

(31) Heusler, K. E. *Corros. Sci.* **1997**, *39*, 1177.